Sustainable Energy Technologies and Assessments 54 (2022) 102811

Contents lists available at ScienceDirect

Sustainable Energy Technologies and Assessments

journal homepage: www.elsevier.com/locate/seta

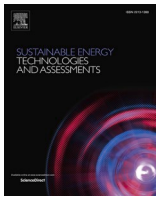

Performance assessment of vertical axis wind turbines (VAWT) through control volume theory

Luis Santamaría *, Katia María Argüelles Díaz, Mónica Galdo Vega, José González Pérez, Sandra Velarde-Suárez, Jesús Manuel Fernández Oro

Fluid Mechanics Area, Department of Energy, University of Oviedo, C/Wifredo Ricart s/n, Gijon, Asturias 33204, Spain

ARTICLE INFO

Keywords:
Vertical axis wind turbine
VAWT
Wind tunnel
Performance characterization
Control volume theory

ABSTRACT

Renewable technologies are the focus of today's energetic scenario. In this context, vertical axis wind turbines (VAWT) have been attracting interest in the last decade as they emerge as good candidates for urban applications and deep-water, multi-megawatt, offshore projects. Nevertheless, their current development state is still limited. Wind tunnel testing is one of the most important tools for their study, but involves high infrastructure costs, which lead to an important downscaling of the prototypes and the consequent problems associated. This work presents the formal development and use of an alternative methodology for characterization of turbine thrust, torque and performance without contact, using data from flow measurements. This is achieved by applying Control Volume (CV) theory which overcomes the typical mechanical issues derived from small-scale prototypes. Complete inlet pressure and wake velocity measurements have been performed and are presented here. From these measurements, turbine thrust, torque and performance have been obtained through CV theory, revealing good agreement with previous experimental data.

Introduction

The global awareness for the 17 Sustainable Development Goals (SDG), where climate action and demographic sustainability are basic pillars, is driving international governments to strongly support renewable energies, economically, legislatively, and politically. However, to meet the ambitious objectives being raised, as achieving net zero emissions by 2050, a massive effort is still needed. Conventional wind power and solar photovoltaic are the technologies currently leading the renewable scenario, with the focus on upscaling. However, with the incoming addition of hydrogen and other grid stabilization and/or energy storage technologies, alternative power generation technologies may still have a role in decarbonization. Furthermore, poly-generation and integrated technology approaches are becoming more common every day, not only in the industrial sector [1] but also in the residential one [2]. Therefore, in this framework, these alternative power generation technologies can find synergies and provide interesting and cost-effective solutions.

In this context vertical axis wind turbines (VAWT) have been receiving increased attention in the last decade, with deep water offshore and urban environments as their main applications. However, their aerodynamics are far complicated and there is still a lack of agreement in a best reference rotor design [3]. Hence, despite their interesting advantages, there is an important lack of real-scale projects, especially in the offshore setting [4]. In the urban application, were there is a small, but stablished, market for these turbines, the biggest setback is the low quality of the wind resource [5]. Thus, one of the latest trends in this field is flow augmentation, achieved either with devices as deflectors or wind lens, or taking advantage of architectural features [6]. Nevertheless, these devices, as well as the turbines are still in development and more research is needed to obtain competitive products.

Wind tunnel testing is vital for the study of this technology, both for the validation of models and simulations and for enhancing the understanding of the flow interactions, which ultimately produce the power output. However, there are some intrinsic problems derived from downscaling that conventional testing methodologies strive to overcome. Mainly, the torque measurement with torquemeters [7] or passive/resistant devices (Prony or electromagnetic brakes [8,9]) increases the mechanical resistance, thus compromising the testable operative ranges. Though sophisticated control systems have been proposed to measure positive torque gradients for the torque-speed ratio curve [10], important restrictions still arise at low power regimes. Therefore, the

* Corresponding author.
E-mail address: santamarialuis@uniovi.es (L. Santamaría).

https://doi.org/10.1016/j.seta.2022.102811
Received 20 May 2022; Received in revised form 22 September 2022; Accepted 28 September 2022
Available online 7 October 2022

Nomenclature

ADM	Active driving mode
b	Wind tunnel test section width
c	Turbine blade airfoil cord
C_P	Power coefficient $\left(\frac{2\omega T_{aero}}{\rho D H v_\infty^3}\right)$
CV	Control Volume
D	Turbine diameter
$\vec{F}$	Acting forces on the fluid
F_w	Frictional shear forces on the tunnel sidewalls (wall)
F_x	Thrust force
h	Wind tunnel test section height
H	Turbine blade Span
I_{x_i}	Turbulent intensity for the streamwise component, in position i
k	Turbulent kinetic energy
$\dot{m}$	Mass flow rate
$\vec{n}$	Normal vector of control surface
N	Number of blades
p_i	Static pressure in position i
p_i'	Fluctuating term of the static pressure in position i
P_i	Averaged term of static pressure in position i
PDM	Passive driving mode
Q_i	Volumetric flow rate in position i
R	Turbine radius
S	Control surface
t	Instant of time
$\vec{t}_i$	Time vector associated to a variable in position i
T	Time period
T_{aero}	Aerodynamic torque
u_i	Streamwise component of total (averaged plus fluctuating) velocity in position i
u_i'	Fluctuating term of the streamwise component of the velocity
U_i	Streamwise component of averaged velocity in position i
v_i	Transversal component of total (averaged plus fluctuating) velocity in position i
v_i'	Fluctuating term of the transversal component of the velocity
$\vec{v}_i$	Averaged wind velocity measured in position i
v_∞	Reference wind velocity ($\vec{v}_1$)
V_i	Transversal component of averaged velocity in position i
$\dot{W}_{vis}$	Viscous drag energy losses in the walls
$\dot{W}_{shear}$	Shear losses in the walls
$\dot{W}_T$	Mechanical energy of the turbine
x	Streamwise direction
y	Transversal direction
Z	Vertical coordinate of measurement positions
α_2	Averaged wind velocity angle in a point of the turbine section outlet (near wake)
ΔP_{i-i}	Pressure difference between different i positions
λ	Tip-speed ratio $\left(\frac{\omega R}{v_\infty}\right)$
ρ	Air density
σ	Turbine solidity $\left(\frac{2Nc}{D}\right)$
τ_i	Shear stress in position i
ω	Turbine rotational speed
0	Position 0, wind tunnel settling chamber
1	Position 1, wind tunnel nozzle outlet
1′	Position 1′, turbine section inlet
2	Position 2, turbine section outlet
$-mid$	Referred to a variable measured in the midplane (Z = 0)
$-gap$	Referred to a variable measured in the center of the gap between the turbine and the floor of the test section (Z = −0.75H)

development of alternative methodologies which are able to avoid these difficulties is inherently interesting.

This work presents an alternative methodology based on performance assessment without contact, obtained from the study of the flow. This alternative methodology is of special interest in set-ups which have a confined configuration or the previously mentioned flow augmentation devices, as well as for studies which are centered in flow visualization techniques as PIV [11]. In both cases, active driving mode (ADM) tests can be applied, producing an equivalent flow behavior to the conventional passive driving mode (PDM) [12,13]. This has the advantage of avoiding cut-in problems and other issues derived from the low available torque with respect to the set-up mechanical losses. Then, carrying out a very affordable number of experimental flow measurements, sufficient data is obtained allowing the application of Control Volume (CV) theory.

Although specifically developed for research environments at the laboratory, the methodology can be applied for real-scale turbines. However, significant difficulties, like the proper definition of control volume or the cost-effective extension of the measurement rakes, discourages its application in favor of a direct mechanical characterization of the turbine performance.

Up to the authors' knowledge on open literature, this is the first time that CV theory is used to provide valuable results for the experimental characterization of VAWTs performance at lab scale. When small-scale prototypes have to be tested in research facilities, the direct determination of mechanical variables for performance measurement can be an issue. Alternatively, aerodynamic variables can be better measured and CV theory employed as a feasible option to complete the mechanical and power balance of the turbine at a convenient cost. In this paper, the methodology described reveals how a moderate number of experimental measurements is sufficient to obtain the performance curve with a reasonable precision. Moreover, a detailed analysis is performed on uncertainty control to check the validity of the method and foresee critical variables requiring especial accuracy.

This work presents a successful application of this methodology to a VAWT wind tunnel set-up described in section 2 and includes the formal development of the control volume theory analysis (section 3). The results from the experimental flow measurements, which serve as basis for its application, are shown in section 4, whereas results from the application of CV theory are exposed and discussed in section 5. Finally, conclusions are drawn, and future works are proposed in section 6.

Experimental set-up and measurements

For this investigation, a specific set-up was designed and arranged in the facilities of the Fluid Mechanics Area of the University of Oviedo. The experiments were performed in the "XAWT" (Xixón Aeroacustic Wind Tunnel), which is a medium size, closed-loop wind tunnel powered by a 30 kW axial fan. The test chamber is anechoic with a cross-section area of 4.45x2.80 m^2 and 4.2 m in length. Fig. 1a), displays a general view of the facility. Velocities up to 22 m/s can be achieved for a mean turbulence intensity around 0.7 % in the test section of 1.15x1 m^2; additional data can be found in [14]. A semi-confined environment is used to enclose the vertical axis turbine, so the dimensions of the test section are preserved towards the exit (extension of 1.7 m). A detailed diagram of the layout of the test chamber with the turbine enclosure is

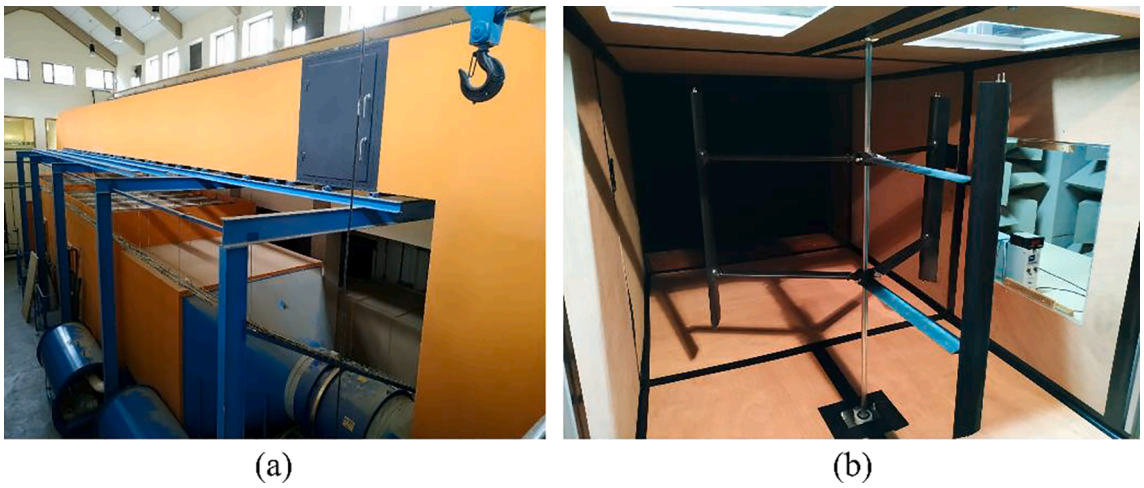

Fig. 1. a) Picture of general overview of the wind tunnel. b) Turbine prototype inside the test section of the wind tunnel.

found later in Fig. 2.

For this research, preliminary aerodynamic measurements of an H-rotor VAWT, performed for a previous work [15], are used in combination with some additional data. To evaluate the performance of the turbine, the authors have recently developed and presented a novel methodology based on active driving mode tests (ADM). This methodology is able to overcome the intrinsic problems from downscaling in a lab environment, assuring good results with remarkable agreement to equivalent CFD simulations. More details can be found in [16]. Precisely, those results are used now as a reference to analyze the outcome of the present work.

The studied turbine was designed for urban environments [17] and it is composed of 3 straight blades (N) with airfoil profile DU 06-W-200, each of them supported by two airfoil-shaped struts with the EPPLER 863 profile (for minimum drag). The dimensions of the scaled prototype are: 0.8 m of diameter (D), 0.6 m of span (H) and 0.067 m of airfoil cord (c), corresponding to a solidity ($\sigma = 2Nc/D$) of 0.5 and aspect ratio (H/D) of 0.75. Fig. 1b), shows the turbine prototype inside the test section of the wind tunnel.

Regarding instrumentation, several pressure transducers were used in combination with pressure tabs to measure static pressures and/or with probes to measure wind velocity. In particular, a digital, differential pressure manometer has been used to measure the inlet velocity, from the pressure difference between the settling chamber and the nozzle outlet. Due to the contraction ratio of 16:1 in the nozzle, the wind velocity in the settling chamber is assumed negligible. For all the experimental dataset, a nominal test velocity of 7.5 m/s has been fixed. Two additional digital manometers were used to measure mean static pressure differences between position 1 and 1′ and between position 1 and 2 (see Fig. 2). A pitot tube was used in the center of the test section at position 1′ to obtain the streamwise velocity upstream of the turbine. Finally, a tailor-made 3-hole pressure probe ("Cobra" type) was used in position 2 to measure in-plane velocity components of the horizontal wake. This pressure probe has been previously developed and tested by members of the research team in precedent works [18,19] and provides a wide angular range of ± 80 deg. This significant feature, and the inherent characteristics of the probe, make it an exceptional tool for this kind of measurements. The Cobra probe is mounted in a positioning system which allows an easy and precise transversal displacement to measure accurately the wake velocity profile. A figure featuring the positioning system and the Cobra probe can be found in the supplementary material accompanying this article.

The measurements were performed in 3 stages. Firstly, the upstream velocity was measured with the pitot tube for 5 different tip-speed ratios ($\lambda = \frac{\omega R}{v_\infty}$, where λ is the tip-speed ratio, ω is the rotational speed of the turbine, R is the radius and v_∞ is the reference wind velocity v_1). To

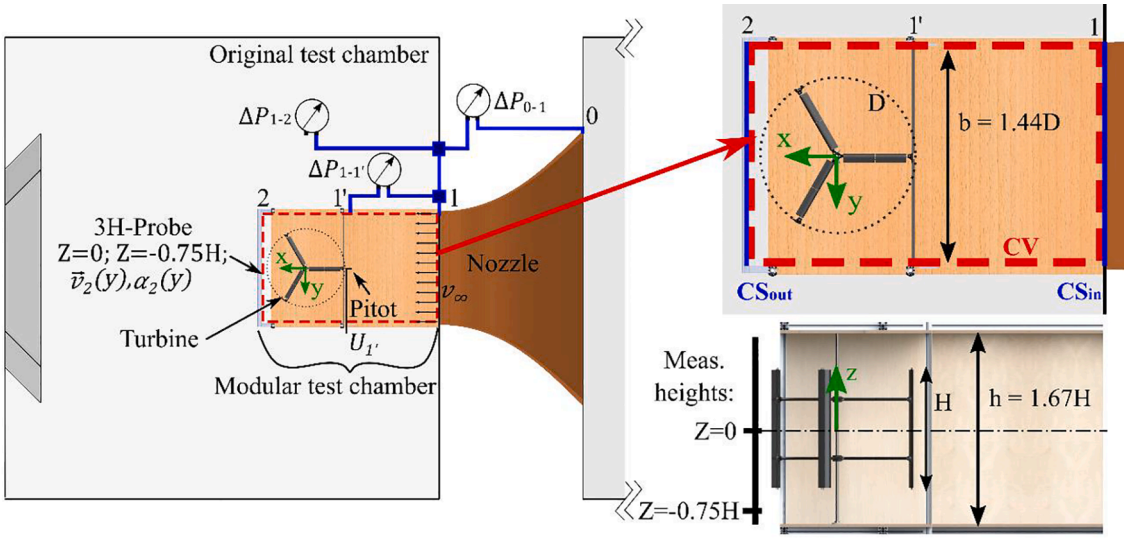

Fig. 2. Three-bladed H-VAWT installed inside an hybrid modular enclosure for the test chamber of the XAWT wind tunnel.

avoid any downstream interferences, these single measurements were completed independently, removing the pitot afterwards. Secondly, in order to obtain a detailed insight on the performance and aerodynamic behavior of the turbine, intensive measurements were performed for 9 different tip-speed ratios at both inlet and outlet midspan sections of the enclosure. The inlet wind velocity (v_1) was kept constant, while the rotational velocity was modified using active driving mode by means of a DC motor. For each tip-speed ratio, meantime wake velocities and incidence angles were measured transversally in the mid-plane at 39 positions (3 cm resolution approximately). While these measurements were obtained, both pressure differences $\Delta P_{1-1'}$ and ΔP_{1-2}, as well as the inlet velocity, have been also recorded, and time-averaged later. Finally, the procedure is repeated placing the cobra probe in the middle of the lower gap between the turbine tip and the enclosure end-wall, which corresponds to a height of Z = − 0.75H below the mid-plane. A complete diagram of the set-up layout and the measurement positions is included in Fig. 2. The uncertainties of the instrumentation used in this work have been detailed in a table included in the supplementary material accompanying this article.

The complete set-up used allows the application of Control Volume (CV) theory in the dashed-red volume defined in Fig. 2. The next section presents in detail the formal development and analysis of this procedure.

Control volume theory

Integral relations obtained from control volume theory can be applied over a turbomachine to evaluate its performance in terms of torque, power consumption and exerting forces. Using the Reynolds transport theorem, balances of mass flow, linear and angular momentum, and energy can be established in multirow environments over integral flow quantities for that purpose. Alternatively, the direct integration of differential balances within the rotor domain provides equivalent formulations for the estimation of the machine performance [20].

Despite it is usually considered as a preliminary approach for the analysis of the internal flow in turbomachinery, CV has been used successfully by several authors to obtain valuable results for both axial and centrifugal geometries [21–24]. Note that a precise analysis requires the inclusion of centrifugal, Coriolis, viscous and blade forces acting in an unsteady fashion, though unsteady components are usually not included in the framework. This has been quite controversial since the demonstration of the necessity of unsteady flow in turbomachines [25], but generally circumvented using CV surfaces outside the blades' vicinity. Time-averaging can also be employed to retrieve the mean-time performance of the turbomachinery, thus introducing additional terms that must be addressed conveniently.

Mass conservation

In the case of the VAWT under study, the control volume depicted in Fig. 2 has been defined for further consideration. Inlet and outlet sections are denoted as (1) and (2) in the figure, with the CV encapsulating all the adjacent blade walls and other solid boundaries. Note that the vertical axis responsible for the turbine rotation corresponds to the axial direction (z-coordinate).

Despite of the cylindrical geometry of the turbine, Cartesian coordinates have been preserved in the following analysis. This is more convenient because the velocity distributions at both inlet and outlet sections are expressed according to the streamwise (u) and transversal (v) directions more easily. After some algebra, the mass conservation equation can be rearranged and expressed as follows:

$$\frac{\partial}{\partial t}\int_{CV}\rho dV + \int_1 -\rho u_1 dS + \int_2 \rho u_2 dS = 0 \tag{1}$$

All the flow variables can be split into average and fluctuating terms due to total unsteadiness (turbulence and periodic wake shedding). In a 2D fashion at the midspan section of the turbine, it is expressed as:

$$u = U + u', v = V + v' \tag{2}$$

where the mean quantities are defined as time averaged variables over a sufficient amount of time.

$$U = \frac{1}{T}\int_t^{t+T} u(t)dt; V = \frac{1}{T}\int_t^{t+T} v(t)dt \tag{3}$$

The time-averaged value of the axial torque can be obtained applying the averaging operator over equation (1). The temporal term is cancelled and taking advantage of the averaging properties, this final expression for incompressible flow is easily found:

$$\int_1 U_1 dS = \int_2 U_2 dS = \int_2 U_{2,gap}\, dS + \int_2 U_{2,mid}\, dS \tag{4}$$

where the outlet section (2) has been split in two different zones (see Fig. 2): the inner region corresponding to midspan locations of the turbine (mid) and the outer region for the vertical clearance with the ducted tunnel (gap).

Linear momentum

In general, the temporal variation of the linear momentum is a consequence of the momentum exchange in the inlet and outlet sections of the control volume, as well as the contribution of both static pressure and shear stress acting on the surfaces of the control volume. A particular form can be retrieved to isolate the force acting on the surfaces of the turbomachinery, resulting in the following classical expression (a nice derivation can be found in [20]):

$$\begin{aligned}\sum \vec{F} = &-\frac{\partial}{\partial t}\int_{CV}\rho\vec{v}\, dV + \int_1 d\dot{m}\, \vec{v}_1 - \int_2 d\dot{m}\, \vec{v}_2 + \int_1\left(-\vec{n}_1 p_1 dS\right)\\ &+\int_2\left(-\vec{n}_2 p_2 dS\right) + \int_1\left(-\vec{t}_1\tau_1 dS\right) + \int_2\left(-\vec{t}_2\tau_2 dS\right)\end{aligned} \tag{5}$$

where $d\dot{m} = \rho\, dS\, \vec{n}\cdot\vec{v}$ represents the differential mass flow rate and 1, 2 are identified as inlet and outlet sections respectively. All the terms in the equation are fully unsteady and stand for the accumulated (integral) contributions of the momentum of static pressures and shear stresses at flow boundaries, as well as the impulse of both incoming and outgoing momentum flow rates. The temporal variation of enclosed kinetic impulse in the CV is also considered. The left-hand side term, $\vec{F}$, includes volumetric forces (i.e. gravitational forces), frictional shear forces on the tunnel sidewalls (wall) and the overall force exerted by the VAWT. Of particular interest is the streamwise component, F_x, acting on the turbomachine since it provides the expression to obtain the axial thrust:

$$F_x + F_w = -\frac{\partial}{\partial t}\int_{CV}\rho u\, dV + \int_1 \left(p_1 + \rho u_1^2\right) dS - \int_2 \left(p_2 + \rho u_2^2\right) dS \tag{6}$$

where the shear stresses on both inlet and outlet sections are vanished. Finally, the time-averaged expression for the linear momentum equation can be obtained considering second-order statistics for the x-velocity component ($\overline{u^2} = \overline{u'^2} + U^2$) and first-order decomposition for the static pressure ($p = P + p'$), resulting:

$$\overline{F_x} = -\overline{F_w} + \int_1 \left[P_1 + \rho\left(U_1^2 + \overline{u_1^2}\right)\right] dS - \int_2 \left[P_2 + \rho\left(U_2^2 + \overline{u_2^2}\right)\right] dS \tag{7}$$

In the present analysis, the inlet section (1) is located far upstream (at × = − 1.85D) to avoid interference effects of the turbine blockage, thus being relevant the longitudinal wall friction in the tunnel. Simple considerations, based on the D'Arcy-Weisbach equation, can be employed to express the tangential force as a function of the pressure

loss in the duct, giving to: $\overline{F_w} = \overline{\Delta P}_{1-1'} hb$, where h and b represent the height and width of the enclosure respectively.

Finally, equation (7) requires the evaluation of the turbulent quantities. It is a common practice to define the turbulent intensity for the streamwise component, I_x, as the ratio between the fluctuating velocities and its mean value according to: $I_x = \sqrt{\overline{u'2}}/U$. Consequently, the final equation to retrieve the time-averaged thrust on the turbine yields:

$$\overline{F_x} = -\overline{P}_{1-1'} hb + \int_1 \left[P_1 + \rho U_1^2\left(1 + I_{x,1}^2\right)\right] dS - \int_2 \left[P_2 + \rho U_2^2\left(1 + I_{x,2}^2\right)\right] dS \tag{8}$$

Though not expressed in eq. (8) for compactness, the outlet integral (2) is also split into the midspan (mid) section and the outer region of vertical clearance (gap) for further evaluation.

Energy equation

The general expression for the exchange of mechanical energy with the turbine (neglecting heat transfer and variations of internal energy and elevation) is expressed as:

$$\begin{aligned} -\dot{W}_T - \dot{W}_{vis} = &-\frac{\partial}{\partial t}\int_{CV}\left(\frac{1}{2}\vec{v}\cdot\vec{v}\right)dV - \int_1\left[\frac{P_1}{\rho} + \frac{1}{2}\vec{v}_1\cdot\vec{v}_1\right]\rho dS\vec{n}_1\vec{v}_1 \\ &+ \int_2\left[\frac{P_2}{\rho} + \frac{1}{2}\vec{v}_2\cdot\vec{v}_2\right]\rho dS\vec{n}_2\vec{v}_2 + \int_1\left(-\vec{t}_1\tau_1 dS\vec{v}_1\right) \\ &+ \int_2\left(-\vec{t}_2\tau_2 dS\vec{v}_2\right) \end{aligned} \tag{9}$$

The triadic tensor terms derived from the time-averaged transport of kinetic energy in the inlet and outlet sections complicates the evaluation of eq. (9). After some manipulation, this contribution (in vectorial form) can be arranged as follows [26]:

$$\left(\frac{1}{2}\vec{v}\cdot\vec{v}\right)\vec{v} = \frac{1}{2}\begin{bmatrix}\left(U^2+V^2\right)U + \left(\overline{u^2}+\overline{v^2}\right)U + \overline{\left(u^2+v^2\right)u'} + 2\left(U\overline{u^2} + V\overline{u'v'}\right) \\ \left(U^2+V^2\right)V + \left(\overline{u^2}+\overline{v^2}\right)V + \overline{\left(u^2+v^2\right)v'} + 2\left(+U\overline{u'v'} + V\overline{v^2}\right)\end{bmatrix}, \tag{10}$$

Following, with the time-averaging operator applied over eq. (9), a reordering of all the terms leads to:

$$\begin{aligned} \overline{\dot{W}_T} = &\underbrace{\int_1\left[P_1 + \frac{1}{2}\rho\left(U_1^2+V_1^2\right)U_1 dS - \int_2\left[P_2 + \frac{1}{2}\rho\left(U_2^2+V_2^2\right)U_2 dS\right]\right]}_{[I]} + \\ &\underbrace{\int_1\frac{1}{2}\left[\left(\overline{u_1^2}+\overline{v_1^2}\right)U_1 + 2\left(U_1\overline{u_1^2} + V_1\overline{u_1'v_1'}\right)\rho dS - \int_2\frac{1}{2}\left[\left(\overline{u_2^2}+\overline{v_2^2}\right)U_2 + 2\left(U_2\overline{u_2^2} + V_2\overline{u_2'v_2'}\right)\right]\rho dS\right]}_{II} + \\ &\underbrace{\int_1\left[\overline{p_1'u_1'} + \frac{1}{2}\rho\overline{\left(u_1^2+v_1^2\right)u_1'}\right]ds - \int_2\left[\overline{p_2'u_2'} + \frac{1}{2}\rho\overline{\left(u_2^2+v_2^2\right)u_2'}\right]dS}_{III} - \underbrace{\overline{\dot{W}}_{shear} - \overline{\dot{W}}_{vis}}_{IV} \end{aligned} \tag{11}$$

In eq. (11), the first term [I] stands for the energy transport of the mean-time mechanical energy of the flow. The second term [II] is associated with the transport of turbulent fluctuations, while the third term [III] is a pure fluctuating term. The final contribution in [IV] accounts for the shear stresses at the flow boundaries and the frictional force at the inlet duct.

Further considerations can be made for the second term in order to reduce the number of variables concerned. In particular, introducing the experimental observation that the stress-intensity ratio $\overline{u'v'}/k$ can be approximated to 0.3 in the log layer of thin shear layer flows [27], being k the turbulent kinetic energy, and assuming isotropic turbulence so $\overline{u^2} = 2k/3$, the turbulent quantities involved in [II] can be expressed as a function of the mean values. Thus, also using the definition of turbulent intensity, it is straightforward to obtain:

$$\begin{aligned} \overline{\dot{W}_T} = &\int_1\left[P_1 + \frac{1}{2}\rho\left(U_1^2+V_1^2\right)\right]U_1 dS - \int_2\left[P_2 + \frac{1}{2}\rho\left(U_2^2+V_2^2\right)\right]U_2 dS \\ &+ \int_1\left[2\,U_1 + a^2V_1\right]\rho U_1^2 I_{x,1}^2 dS - \int_2\left[2\,U_2 + a^2V_2\right]\rho U_2^2 I_{x,2}^2 dS - \overline{P}_{1-1'}Q \end{aligned} \tag{12}$$

where $a^2 = 0.45$ and the third term [III] has been assumed to be negligible [26]. In addition, the energy loss due to the shear stresses at the entrance and exit cross sections of the flow channel in [IV] must usually be ignored in practical applications.

This final equation (12) allows to compute the aerodynamic power of the VAWT as a function of the mean time values of the flow field measured at both inlet and outlet sections. A rough estimation of the turbulent intensity for the streamwise component must also be provided in order to analyze the averaged impact of the flow fluctuations in the aerodynamic power. Moreover, assuming uniform pressure distributions at both sections (at the inlet it is fulfill due to symmetric kinematic conditions at the nozzle discharge, whereas there are atmospheric conditions at the flow discharge), the pressure work can be easily evaluated. Note that only in-plane components have been considered relevant: local variations of out-plane components related to departure from 2D flow in the axial direction (at midspan) and streamwise mixing-out within the turbine enclosure are considered marginal for the evaluation of the turbine power. As before, the integral in section (2) has been divided in the inner (mid) and outer (gap) zones for the evaluation of the velocity distributions measured experimentally.

Measurement results

Upstream velocity and inlet pressure drop

The evolution of the upstream velocity at the turbine inlet, normalized by the incoming velocity, is shown in Fig. 3a). At low tip-speed ratios (from 0.0 to 1.6), streamwise velocity in position 1′ is practically identical to the inlet velocity. Between tip-speed ratios from 1.6 to 2.5 there is a remarkable decrease of roughly 10 % in the velocity value. Note that this result is coherent with previous experimental data evidencing that positive net torque generation starts around a tip-speed ratio of 2 for this rotor design [16]. From 2.5 to 3.5, the velocity drop is slowed down, although a total reduction of almost a 15 % is perceived. This evidence justifies the extension of the inlet section for the control volume and the need for considering the influence of section 1-1′ in the analysis.

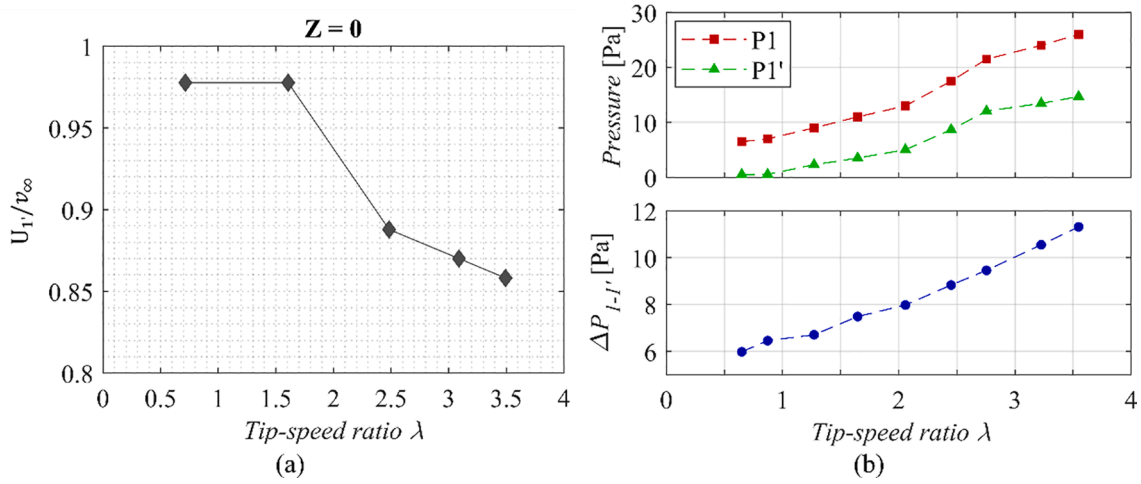

Fig. 3. a) Dimensionless mean velocity in the upstream section (mid-plane height) for 5 different tip speed ratios. b) Manometric pressure at 1 and 1′ and pressure difference for 9 different tip-speed ratios.

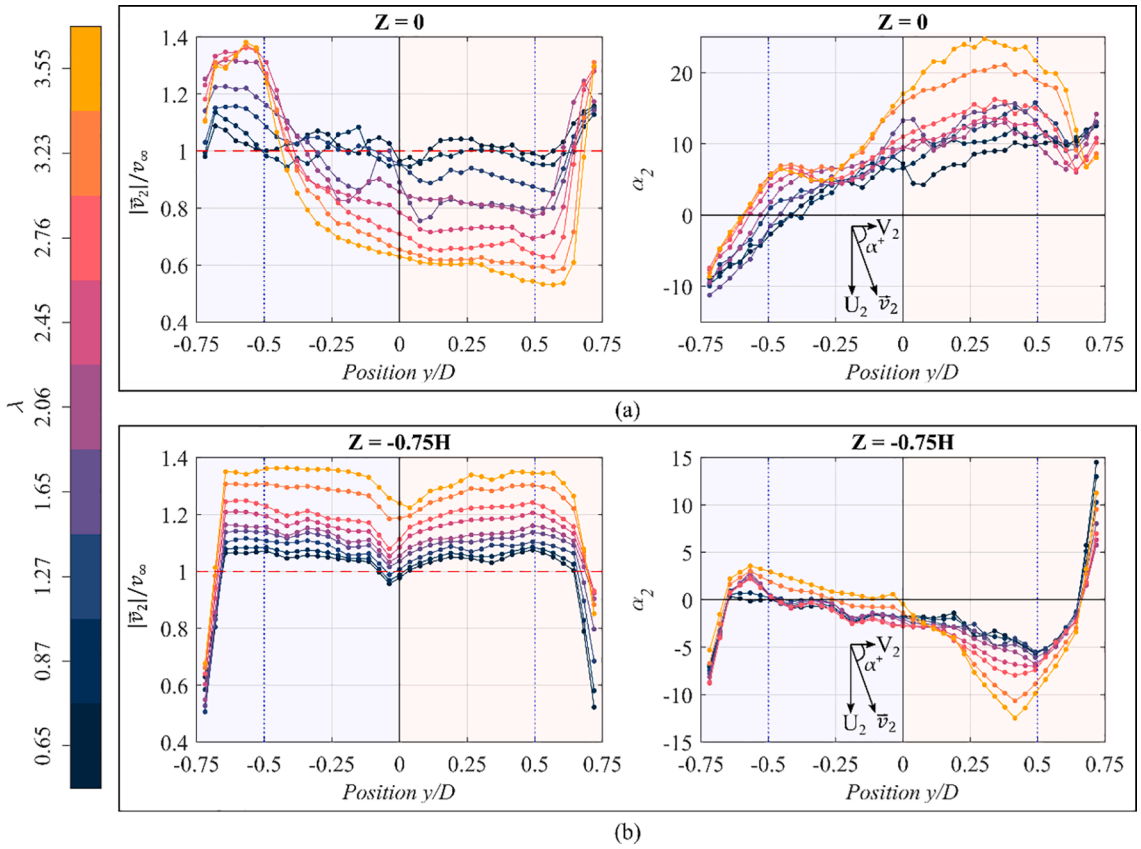

Fig. 4. Transversal distributions of velocity magnitude and flow angle as a function of the tip-speed ratio *a)* measured in the mid-plane of the near wake area. b) measured in the axial gap of the near wake area.

Figure 3b), shows the evolution of the static pressure measured at the turbine inlet for the whole range of tip-speed ratios tested. It is expressed in relative terms (gauge) since the manometric pressure in position 2 (*P2*) is atmospheric (0 Pa). The pressure loss between sections 1 and 1′ increases almost linearly with the tip speed ratio, exhibiting a quite small difference that ranges from 6 to 12 Pa (blue dashed line). The pressure drop across the turbine is quite similar, ranging from 0 to 15 Pa (green dashed line), although its increasing trend somewhat resembles the behavior of the turbine performance curve. Note that the total pressure difference between the inlet and outlet sections of the CV is significant, ranging from 8 to 28 Pa (red dashed line).

Wake velocity profiles

A complete characterization of the wake velocities and in-plane flow angles has been performed transversally in position 2 for the whole range of tip-speed ratios. Fig. 4a) shows the results of the measurements conducted in the mid-plane (Z = 0). The velocity magnitude $\left|\vec{v}_2\right|$, made dimensionless with the inlet velocity, is plotted along the transversal

position over the turbine diameter, in the left graph. Vertical dashed lines indicate the turbine width. The light blue area of the graph corresponds to the zone in which the turbine blade is moving leeward, while the light red area corresponds the windward zone. The velocity distribution for each tip-speed ratio has been colored according to the color-bar scale. There is a progressive increase in the velocity magnitude at the lateral sides, especially in the leeward area. Likewise, in the wake of the turbine there is a remarkable decrease in the velocity magnitude, particularly in the windward area in which a 50 % reduction with respect to the inlet velocity is observed at the highest tip-speed ratio. Regarding the flow angle (right plot), there is a significant increment across the whole range of tip-speed ratios, indicating a progressive enlargement of the transversal component of the velocity that matches the direction of rotation of the turbine. This angle increase is mostly appreciated in the windward area.

In Fig. 4b), similar velocity and angle profiles are presented, but now corresponding to the central line of the gap (axial clearance, $Z = -0.75$) between the turbine and the wind tunnel.

The overall magnitude of the velocity in this section is quite constant, except for the central part, which is probably affected by the shaft shadow. On the sides, the shear layer produced by the wind tunnel walls is easily identifiable. As it can be noted, there is a remarkable increase of the gap velocity, achieving almost 140 % of the inlet velocity. Also, there is a noticeable increase in the magnitude of the angle, especially in the windward area, indicating a widening of the stream.

Control volume theory results

Steady measurements shown in previous section have been employed to evaluate the integral relationships derived from CV theory for the present set-up (equations (4), (8) and (12)). Unsteady contributions due to turbulence have been introduced assuming characteristic turbulent intensity levels for both mid-span and gap zones. These values were roughly estimated based on auxiliary hot-wire measurements and results from CFD simulations. In particular, an averaged turbulence level of 0.7 % has been assumed at the control volume inlet, while an increased turbulent intensity of a 12 % was employed at the turbine exit, and a 2 % in the gap section. Although unsteady effects can be relevant and should not be omitted, it is demonstrated that a precise quantification of the turbulence level is marginal for a correct application of the method. In following section 5.4, other factors are shown to have a critical impact for a sufficient characterization of the turbine performance.

Mass conservation

Two approaches have been compared to assess the minimum number of measurements required for a representative application of the control volume theory. Firstly, applying mass conservation (eq. (4)), the flow rate in the gap region of the outlet section can be derived from the measurements at the mid-plane. Following, this result is compared with the flow rate computed directly from the measurements in the center of the gap clearance (considered representative for the hole gap). Table 1a) shows the flow rates for the different tip-speed ratios measured and the flow rate obtained indirectly from mass balance for the gap area. Likewise, Table 1b) shows the resultant flow rate in section 2 obtained from the use of the gap measurements. Also, the absolute and relative differences in the computed flow rate at the outlet are provided. Note that the maximum flow rate difference is only a 3 %, in the case of the highest tip-speed ratio. Moreover, characteristic discrepancy can be established around 1 % which it is remarkably low to validate the assumption of planar flow.

Linear momentum

Linear momentum equation has been applied to obtain the axial thrust of the turbine. Typically, the direct measurement of aerodynamic forces is a complex task, involving elaborate set-ups where the turbine is installed on a multiple component balance. Moreover, at a lab scale these forces are significantly small, which usually compromises the obtention of a reliable value. Complementary methods for an indirect estimation of the forces in VAWTs prototypes are thus interesting and demanded.

Consequently, both approaches (applying continuity or measuring the gap flow) have been compared for the estimation of the axial thrust using equation (8). The obtained results are shown in Table 2. Thrust forces range from almost 0 to 11 or 14 N (depending on the approach) which are coherent values for this kind of turbine rotor. In addition, the greatest difference in the estimation of the reaction force at the outlet gap is only a 10 % at the highest tip-speed ratio, which it is a quite remarkable result considering the small values of those forces. In this worst case, maximum differences between approaches represent only a couple of N for the overall thrust of the turbine.

Energy equation

Finally, the measured data is employed to evaluate the integral terms of the energy equation to obtain the performance curve of the turbine. Equation (12) provides the aerodynamic power directly, which can be further divided by the rotational velocity to retrieve the aerodynamic torque. The results are compared with the experimental measurements obtained from the application of the ADM methodology in the same set-up [16].

Fig. 5 shows the power coefficient ($C_P = 2\omega T_{aero}/\rho DHv_\infty^3$) versus tip-speed ratio in a non-dimensional form. The same figure in terms of aerodynamic torque versus rotational velocity can be found in the supplementary material accompanying this article. Results derived from the application of mass conservation are plotted with red circles and dotted lines. Likewise, results using the gap measurements are plotted with green squares and dotted lines. The experimental results are represented

Table 1
a) Computed volume flow rates using mid-plane measurements and continuity equation. b) Computed volume flow rates using mid-plane measurements and gap measurements. Absolute and relative differences in computed flow rate at the outlet (position 2).

(a)				(b)			
λ	$Q_1 = Q_2$	Q_{2mid}	Q_{2gap} (Continuity)	Q_{2gap} (meas.)	Q_2	E_{abs}	E_r
[-]	[m^3/s]	[m^3/s]	[m^3/s]	[m^3/s]	[m^3/s]	[m^3/s]	[%]
0.65	8.77	5.33	3.44	3.56	8.89	−0.12	−1.33
0.87	8.76	5.19	3.57	3.60	8.80	−0.03	−0.39
1.27	8.75	5.13	3.62	3.68	8.82	−0.06	−0.71
1.65	8.74	4.89	3.85	3.78	8.68	0.07	0.75
2.06	8.85	5.09	3.76	3.90	8.99	−0.14	−1.57
2.45	8.84	4.81	4.03	4.03	8.84	0.00	−0.02
2.76	8.82	4.53	4.29	4.14	8.67	0.15	1.74
3.23	8.81	4.24	4.57	4.37	8.61	0.19	2.18
3.55	8.79	3.99	4.80	4.53	8.52	0.27	3.03

Table 2
a) Computed thrust forces using mid-plane measurements and continuity equation. b) Computed thrust forces using mid-plane measurements and gap measurements. Absolute and relative differences in computed flow rate at the outlet (position 2).

(a)						(b)			
λ [-]	F_{x1} [N]	$F_{x\ wall}$ [N]	$F_{x2\text{-}mid}$ [N]	$F_{x2\text{-}gap}$ (Continuity) [N]	F_x (Continuity) [N]	$F_{x2\text{-}gap}$ (Measured) [N]	F_x (Measured) [N]	E_{abs} (F_{x2}) [N]	E_{rel} (F_{x2}) [%]
0.65	47.07	−6.86	−24.74	−15.59	−0.12	−16.80	−1.33	−1.21	7.76
0.87	47.65	−7.41	−23.58	−16.74	−0.08	−17.21	−0.55	−0.47	2.81
1.27	49.94	−7.69	−23.25	−17.22	1.78	−17.97	1.02	−0.76	4.36
1.65	52.35	−8.59	−21.58	−19.46	2.72	−18.94	3.24	0.52	−2.67
2.06	56.26	−9.15	−23.70	−18.61	4.79	−20.14	3.27	−1.53	8.22
2.45	60.85	−10.14	−21.79	−21.33	7.59	−21.49	7.44	−0.15	0.75
2.76	65.15	−10.86	−19.81	−24.22	10.27	−22.65	11.84	1.57	−6.48
3.23	68.31	−12.11	−17.91	−27.38	10.91	−25.29	13.00	2.08	−7.63
3.55	70.61	−12.99	−16.29	−30.23	11.10	−27.18	14.15	3.05	−10.09

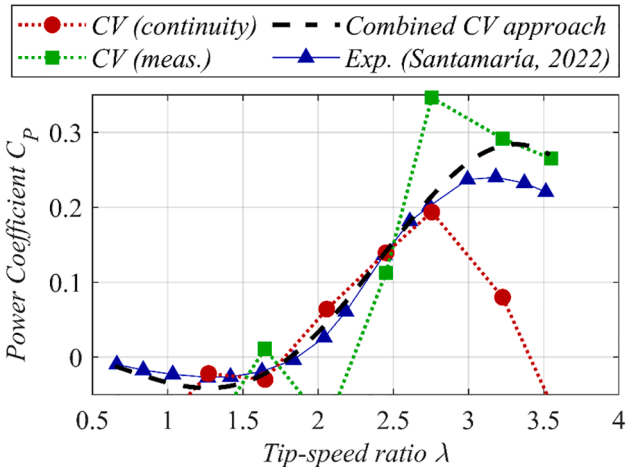

Fig. 5. Computed aerodynamic performance as a function of the tip-speed ratio. Comparison of results from the application of CV theory with experimental measurements.

with blue triangles and continuous lines in the figure.

For low tip-speed ratios (below 1.27, corresponding to 230 rpm), the results obtained with the CV theory are not consistent with the experimental values. Power coefficient and torque values drop severely to high negative values ([-0.1, −0.23] and [-1, −2.2] Nm for the continuity and the gap measurement approaches respectively), revealing that the measured values are excessively small to obtain reliable estimations from the integral relationships. For moderate tip-speed ratios, between 1.27 and 2.76 (505 rpm), the results of the CV theory with the continuity approach perfectly reproduce the experimental curve for both torque and performance coefficient. Alternatively, the CV results using gap measurements present important discrepancies, exhibiting significant oscillations. Finally, in the case of high tip-speed ratios (above 2.76), the results of CV theory using the gap measurements predict the experimental curve beyond the maximum point with high accuracy, while CV results using continuity suffer from a sudden, overestimated drop.

The deviation of the continuity-based CV theory at high tip-speed ratios is produced by the blockage effect of the turbine, which intensifies the relative importance of the gap flow. The moderate-to-low solidity of the turbine prevents this effect to be relevant at low tip-speed ratios. However, when the rotational speed is progressively increased, the apparent flow area in the turbine zone is reduced and a remarkable enlargement in the gap velocity is produced. Because of the limited gap, the increased velocity reduces the flow homogeneity in the spanwise direction. Thus, the mid-plane measurements are not sufficient to describe the outlet flow of the whole turbine span and, hence, the application of the continuity balance is no longer valid.

The fact that the results of the CV approach using gap measurements approximate better the experimental curve at high-tip speed ratios evidences the considerable influence of the gap over the turbine performance. However, this approach is also susceptible of introducing errors, especially at moderate tip-speed ratios, as observed in the points of tip-speed ratio 2.06 and 2.76, clearly out of range. This feature indicates the need for a concise assessment of the relevant variables introducing major uncertainties in the estimation of the turbine performance. A thorough analysis is presented in section 5.4.

To conclude, a performance curve based on CV theory is finally provided using the combined results of both approaches (plotted in Fig. 5 as a dashed, black line). A sum of sine waveforms has been used to blend the different datasets. In general, flow velocities at the gap can be derived from mass conservation to determine the torque and power coefficient curves when positive torque gradients are guaranteed (corresponding to low-to-moderate tip-speed ratios). On the contrary, the gap velocity and flow angle should be measured in case of high tip-speed ratios. The coherence of the results corresponding to very low tip-speed ratios requires further evaluation and ultimately it could be replaced by placing a first point in the origin.

Error transmission and influence

This paper is concluded presenting a detailed assessment of the most critical variables showing a major impact on the CV results. In particular, a thorough empirical analysis has been performed on error transmission and influence over the final performance figures. For that purpose, 1 % and 5 % deviations were applied to the measured variables independently, to evaluate the effect of these deviations in the final results. Special attention is devoted to the pressure and velocity components at both inlet and outlet sections of the control volume. Negative deviations were also applied, obtaining an almost fully symmetrical response, so they are not shown here for simplicity. The errors of the performance coefficients have been reduced to a single value by applying the Euclidean norm, in the following way:

$$\epsilon_r(C_P) = \frac{\|C_P - C_P^{'}\|}{\|C_P\|} = \frac{\sqrt{\sum \left(C_{P_i} - C_{P_i}^{'}\right)^2}}{\sqrt{\sum C_{P_i}^2}} \tag{13}$$

where C_P contains the values of the power coefficient for every tip-speed ratio in the original curve and $C_P^{'}$ are the deviated curves for each deviated variable. This is performed both for the continuity equation approach and the approach using gap measurements. The results for both approaches have been included in Fig. 6.

As expected, small errors in the measurements of the pressure and in the streamwise component of the velocity can cause large errors in the final performance coefficient, thus indicating that these variables are the most critical to the procedure. In the case of the continuity approach, it is shown that errors in the power coefficient estimation can be as high as a 60 % if pressure and velocity measurements are deviated roughly a 5 %

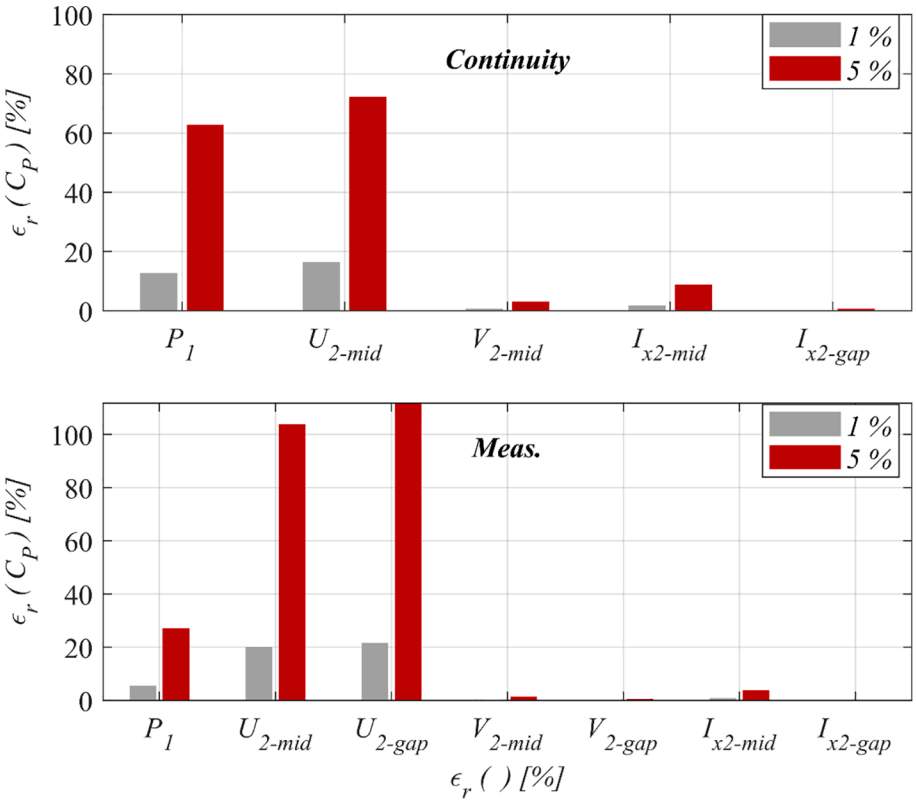

Fig. 6. Relative errors in the estimation of the turbine performance as a function of 1% and 5% errors in the input variables. Comparison between continuity equation and gap measurement approaches.

from its true value. Moreover, the worst situations are observed when the gap velocity is taken from the measurements, though the influence of the pressure is less important in that case. On the other hand, the transversal component of the velocity and the turbulence intensity in the gap have very small relevance, with deviations smaller than 3.1 % and 0.7 % respectively, for the 5 % input deviation and continuity equation approach and even lower in the approach based on gap measurements (1.3 % and 0.03 %). Turbulence intensity in the turbine region has a slightly higher relevance, with lower output than input deviations in the gap-measurements approach, being duplicated in the case of the continuity equation approach. In general, a maximum uncertainty below 1 % in the measured variables is recommended to preserve inaccuracies in the range of a 10 % in the estimation of the performance curve.

Conclusions

In this work, control volume theory has been presented as a useful tool for performance and thrust assessment of vertical axis wind turbines using flow measurements. The methodology has been formally developed from the theory and applied to a real set-up.

This methodology is of particular interest for the characterization of lab-scale prototypes, where the direct measurement of mechanical variables can be problematic at low power regimes. With a detailed measurement and analysis of the evolution of inlet pressures and outlet wake velocities, quality data has been provided and shown valid for the application of control volume theory.

The range of application of this methodology is found to be limited to the positive torque generation region, i.e. from $\lambda = 2.06$ on in the present turbine set-up, due to the quite low magnitude of the measured values at very low tip-speed ratios. From low to moderate tip-speed ratios an approach based on the continuity equation provides the best results. From moderate to high tip-speed ratios, the assumption of planar flow decays due to the increased blockage. Hence, additional measurements are needed to obtain a more representative characterization of the outlet flow, which allows a more precise evaluation of the torque and performance in this range.

To conclude, remarkable agreement has been found between the control volume theory results and experimental torque and performance measurements, validating the procedure. Likewise, thrust results are found coherent and in range. Nevertheless, high precision is needed in the measurement of the velocities, as they have been identified as the most critical variables to the application of the methodology. In particular, deviations of a 5 % in the velocity measurements may lead to a 60 % error in the correct estimation of the power coefficient. Thus, overall measurement uncertainty should be kept below 1 % to preserve maximum inaccuracies in the range of a 10 % for the performance curve.

Finally, as future works, the use of control volume theory in set-ups different to the one studied here is proposed, being particularly interesting the application of the procedure to wind turbine array testing.

CRediT authorship contribution statement

Luis Santamaría: Conceptualization, Investigation, Data curation, Writing – original draft. **Katia María Argüelles Díaz:** Investigation, Project administration, Writing – review & editing. **Mónica Galdo Vega:** Investigation. **José González Pérez:** Visualization. **Sandra Velarde Suárez:** Supervision, Funding acquisition. **Jesús Manuel Fernández Oro:** Formal analysis, Methodology, Writing – review & editing, Supervision.

Declaration of Competing Interest

The authors declare that they have no known competing financial interests or personal relationships that could have appeared to influence the work reported in this paper.

Data availability

Data will be made available on request.

Acknowledgements

The authors wish to thank the financial support of the Spanish Ministry of Economy, Industry and Competitiveness for the R + D Project entitled "Development and Construction of Vertical Axis Wind Turbines for Urban Environments" (DEVTURB) – Ref. ENE2017-89965-P, under the National Plan for Scientific and Technical Research and Innovation.

The grant provided by the Principality of Asturias for the support of Research Activities, funded by the Institute for Economic Development (IDEPA) under reference GRUPIN IDI/2018/000205 is also gratefully acknowledged.

Additionally, the support given by the University Institute for Industrial Technology of Asturias (IUTA) and the City Hall of Gijón, through the financed project SV-18-GIJON-1-05, is also recognized.

Finally, the authors would like to acknowledge the contribution of Prof. Bruno Pereiras for his advice and support during the measurement campaign.

Appendix A. Supplementary data

Supplementary data to this article can be found online at https://doi.org/10.1016/j.seta.2022.102811.

References

[1] Costa M, Buono A, Caputo C, Carotenuto A, Cirillo D, Costagliola MA, et al. The "INNOVARE" project: Innovative plants for distributed poly-generation by residual biomass. Energies 2020;13. https://doi.org/10.3390/en13154020.
[2] Pinto ES, Serra LM, Lázaro A. Optimization of the design of polygeneration systems for the residential sector under different self-consumption regulations. Int J Energy Res 2020;44:11248–73. https://doi.org/10.1002/er.5738.
[3] Barnes A, Marshall-Cross D, Hughes BR. Towards a standard approach for future Vertical Axis Wind Turbine aerodynamics research and development. Renew Sustain Energy Rev 2021;148:111221. https://doi.org/10.1016/j.rser.2021.111221.
[4] Hand B, Cashman A. A review on the historical development of the lift-type vertical axis wind turbine: From onshore to offshore floating application. Sustainable Energy Technol Assess 2020;38. https://doi.org/10.1016/j.seta.2020.100646.
[5] Kumar R, Raahemifar K, Fung AS. A critical review of vertical axis wind turbines for urban applications. Renew Sustain Energy Rev 2018;89:281–91. https://doi.org/10.1016/j.rser.2018.03.033.
[6] Zhao Z, Wang D, Wang T, Shen W, Liu H, Chen M. A review: Approaches for aerodynamic performance improvement of lift-type vertical axis wind turbine. Sustainable Energy Technol Assess 2022;49:101789. https://doi.org/10.1016/j.seta.2021.101789.
[7] Castelli MR, Ardizzon G, Battisti L, Benini E, Pavesi G. Modeling Strategy and Numerical Validation. In: Proceedings of the ASME 2010 International Mechanical Engineering Congress & Exposition; 2010. p. 1–10.
[8] Mertens S, Van Kuik G, Van Bussel G. Performance of an H-Darrieus in the skewed flow on a roof. J Solar Energy Eng, Trans ASME 2003;125:433–40. https://doi.org/10.1115/1.1629309.
[9] Du L, Ingram G, Dominy RG. Experimental study of the effects of turbine solidity, blade profile, pitch angle, surface roughness, and aspect ratio on the H-Darrieus wind turbine self-starting and overall performance. Energy Sci Eng 2019;7:2421–36. https://doi.org/10.1002/ese3.430.
[10] Edwards JM, Angelo Danao L, Howell RJ. Novel experimental power curve determination and computational methods for the performance analysis of vertical axis wind turbines. J Solar Energy Eng, Trans ASME 2012;134:1–11. https://doi.org/10.1115/1.4006196.
[11] Arpino F, Cortellessa G, Scungio M, Fresilli G, Facci A, Frattolillo A. PIV measurements over a double bladed Darrieus-type vertical axis wind turbine: A validation benchmark. Flow Measurement and Instrumentation 2021;82. 10.1016/j.flowmeasinst.2021.102064.
[12] Dou B, Yang Z, Guala M, Qu T, Lei L, Zeng P. Comparison of different driving modes for the wind turbine wake in wind tunnels. Energies 2020;13. https://doi.org/10.3390/en13081915.
[13] Araya DB, Dabiri JO. A comparison of wake measurements in motor-driven and flow-driven turbine experiments. Exp Fluids 2015;56:1–15. https://doi.org/10.1007/s00348-015-2022-7.
[14] Rodríguez Lastra M, Fernández Oro JM, Galdo Vega M, Blanco Marigorta E, Santolaria MC. Novel design and experimental validation of a contraction nozzle for aerodynamic measurements in a subsonic wind tunnel. J Wind Eng Ind Aerodyn 2013;118:35–43. https://doi.org/10.1016/j.jweia.2013.04.008.
[15] Santamaría L, María K, Díaz A, Pereiras B, Vega MG, Pérez JG, et al. Preliminary flow measurements of a small-scale, vertical axis wind turbine for the analysis of blockage influence in wind tunnels. AICFM16 J Phys Conf Ser 2022. https://doi.org/10.1088/1742-6596/2217/1/012039.
[16] Santamaría L, Fernández Oro JM, Argüelles Díaz KM, Meana-Fernández A, Pereiras B, Velarde-Suárez S. Novel methodology for performance characterization of vertical axis wind turbines (VAWT) prototypes through active driving mode. Energy Convers Manage 2022;258:115530. https://doi.org/10.1016/j.enconman.2022.115530.
[17] Meana-Fernández A, Solís-Gallego I, Fernández Oro JM, Argüelles Díaz KM, Velarde-Suárez S. Parametrical evaluation of the aerodynamic performance of vertical axis wind turbines for the proposal of optimized designs. Energy 2018;147:504–17. https://doi.org/10.1016/j.energy.2018.01.062.
[18] Díaz KMA, Oro JMF, Marigorta EB. Extended angular range of a three-hole cobra pressure probe for incompressible flow. J Fluids Eng, Trans ASME 2008;130:1014011–6. https://doi.org/10.1115/1.2969457.
[19] Argüelles Díaz KM, Fernández Oro JM, Blanco Marigorta E, Barrio PR. Head geometry effects on pneumatic three-hole pressure probes for wide angular range. Flow Meas Instrum 2010;21:330–9. https://doi.org/10.1016/j.flowmeasinst.2010.04.004.
[20] Vavra MH. Aero-thermodynamics and flow in turbomachines. New York: John Wiley & Sons, Inc.; 1960.
[21] Selig MS, McGranahan BD. Wind tunnel aerodynamic tests of six airfoils for use on small wind turbines. 2004. 10.2514/6.2004-1188.
[22] Yan P, Chu N, Wu D, Cao L, Yang S, Wu P. Computational fluid dynamics- based pump redesign to improve efficiency and decrease unsteady radial forces. J Fluids Eng, Trans ASME 2017;139. https://doi.org/10.1115/1.4034365.
[23] Olasek K, Karczewski M. Velocity data-based determination of airfoil characteristics with circulation and fluid momentum change methods, including a control surface size independence test. Exp Fluids 2021;62:1–21. https://doi.org/10.1007/s00348-021-03193-9.
[24] Kaupert KA. An evaluation of impeller blade torque during an impeller-diffuser interaction. J Fluids Eng, Trans ASME 2004;126:960–5. https://doi.org/10.1115/1.1839929.
[25] Dean RC. On the necessity of unsteady flow in fluid machines. J Basic Eng 1959;81. https://doi.org/10.1115/1.4008350.
[26] Young J, Tian F-B, Liu Z, Lai JCS, Nadim N, Lucey AD. Analysis of unsteady flow effects on the Betz limit for flapping foil power generation. J Fluid Mech 2020;902. https://doi.org/10.1017/jfm.2020.612.
[27] Durbin PA, Petterson Reif BA. Statistical theory and modelling for turbulent flows. Chinchester: John Wiley & Sons, Inc.; 2011.